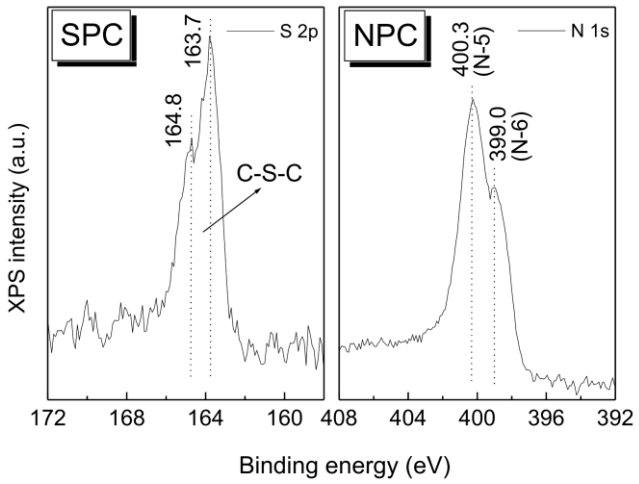

Supplementary Figure 1 | XPS indicates 13.3 atomic% of S in the SPC precursor and 22.4 atomic% of N in the NPC precursor, while the resulting SPC and NPC then had 8.1 atomic% of S content and 6.2 atomic% of N content, respectively. The S_{2p} and N_{1s} XPS peaks taken from the SPC and NPC. The S_{2p} core splits into two main peaks 163.7 ($2p_{3/2}$) and 164.8 eV ($2p_{1/2}$), which corresponds to thiophenic sulfur atoms incorporated into the porous carbon framework via the formation of C-S-C bond. The N_{1s} reflects two different chemical environments: pyridinic nitrogen (N-6) and pyrrolic nitrogen (N-5) atoms. The carbonization of poly(acrylonitrile) is a process that is well-studied in making carbon fiber.

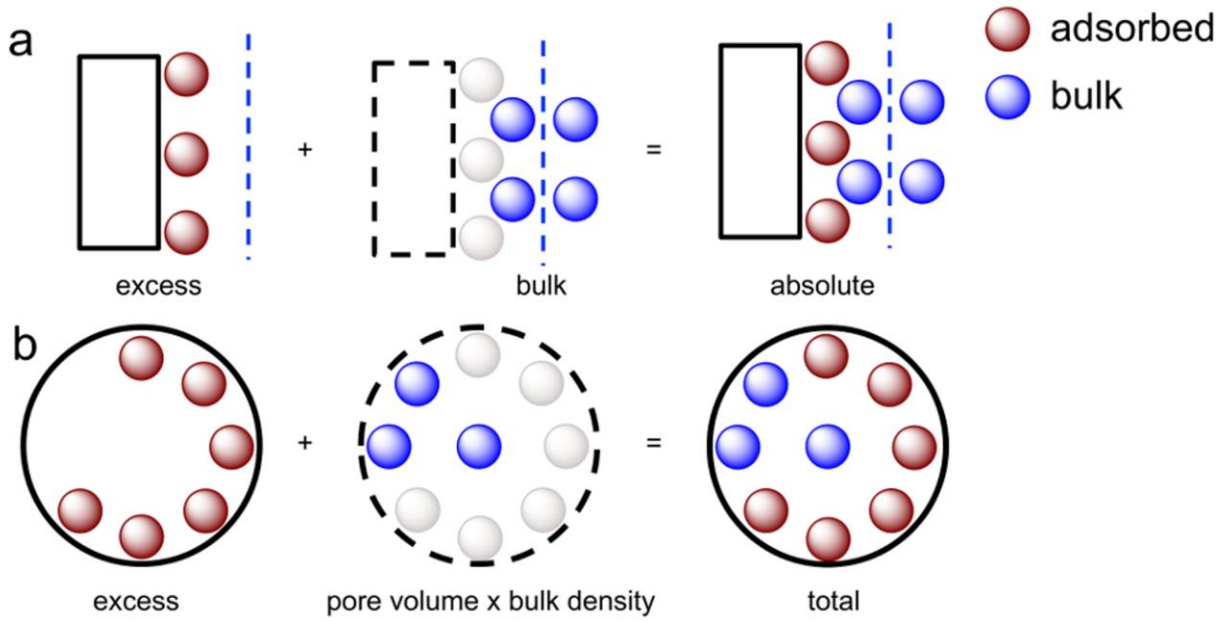

Supplementary Figure 2 | Pictorial description of excess and absolute uptake (a) adapted from reference *1*. The blue dashed line indicates the Gibbs dividing surface. It divides the free volume into two regions in which gas molecules are either in an adsorbed or bulk state. Total uptake (b) is often used as an approximation for absolute uptake for microporous materials with negligible external surface area.

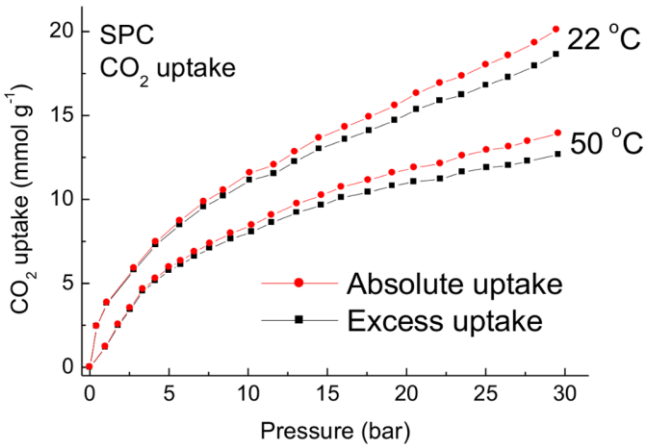

Supplementary Figure 3 | CO_2 uptake on the SPC. Comparison of absolute uptake and excess uptake at 22 and 50 °C which exemplifies the small differences over this pressure and temperature range.

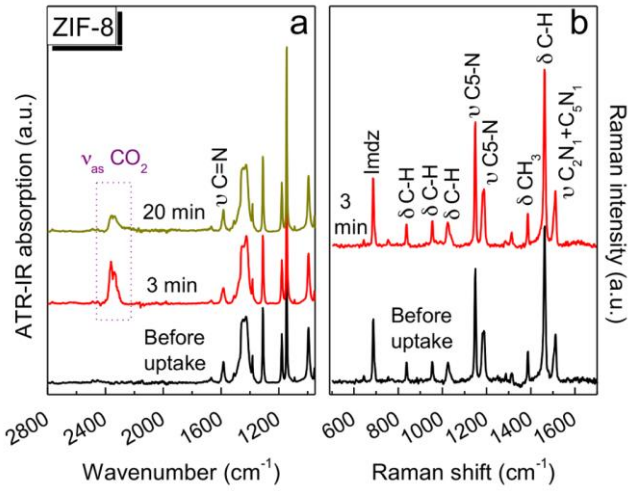

Supplementary Figure 4 | (a) ATR-IR and (b) Raman spectra for the ZIF-8 before and after CO_2 sorption at 10 bar. All spectra were recorded 3 and 20 min after the ZIF-8 sorbent was returned to ambient pressure at room temperature.

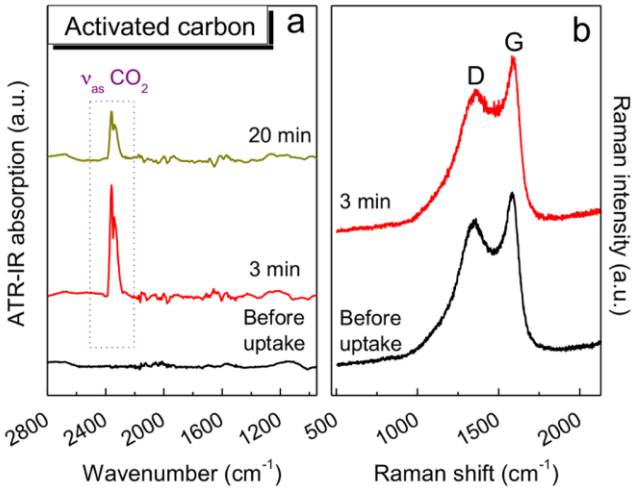

Supplementary Figure 5 | (a) ATR-IR and (b) Raman spectra for the activated carbon before and after CO_2 sorption at 10 bar. Spectra were taken 3 min and 20 min after the activated carbon was returned to ambient pressure at room temperature.

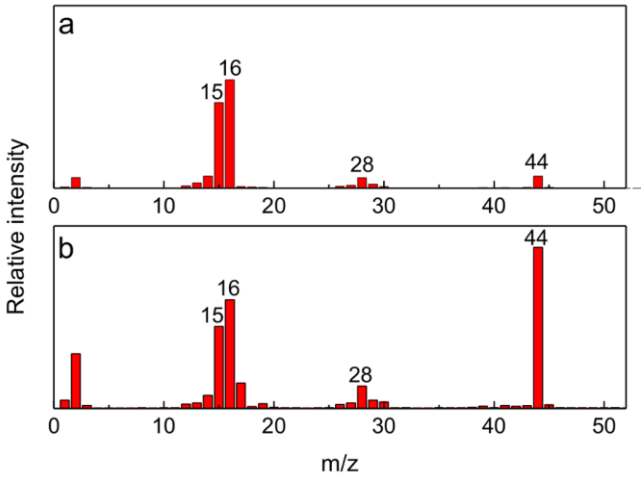

Supplementary Figure 6 | MS data. (a) MS was taken while the system was being pressurized with a premixed gas of CO_2 in natural gas during the uptake process. (b) MS was recorded while the premixed gas-filled SPC was desorbing from 30 bar. The mixed gas was purchased from Applied Gas Inc.

Supplementary Table 1. Heat of CO_2 sorption determined here vs. literature values.

	Q_{CO2} (kJ mol^{-1})	Comparison with reference
SPC	57.8	59.0[3]
Activated carbon	28.4	28.9[4]
Zeolite 5A	31.2	33.7[5]
ZIF-8	25.6	27.0[6]

Supplementary Notes

Supplementary Note 1. Conversion of excess uptake to absolute uptake

Total uptake includes all gas molecules in the adsorbed state, which is the sum of the experimentally measured excess uptake and the bulk gas molecules within the pore volume (Supplementary Figure 2). For microporous materials with negligible external surface area, the total uptake is often used as an approximation for absolute uptake and could be represented in the following equation[1]:

$$N_{total} \approx N_{abs.} = N_{ex.} + V_p \bullet \rho_{bulk}(P,T) \quad (1)$$

where V_p is the pore volume of porous material and ρ_{bulk} is the density of gas in the bulk phase at given pressure and temperature. In the case of SPC, the pore volume was determined to be 1.01 $cm^3\ g^{-1}$ by N_2 adsorption isotherm at 77 K (BET analysis). The CO_2 density changes from 0.00180 to 0.06537 g cm^{-3} in the pressure range between 1 and 30 bar at 22 °C and 0.00164 to 0.05603 g cm^{-3} at 50 °C.

Supplementary Note 2. Determination of the heat of CO_2 sorption (Q)

Clausius-Clapeyron equation[2]:

$$\left(\frac{\partial\, ln\, P}{\partial\, T}\right)_\theta = \frac{Q}{RT^2} \quad (2)$$

Where θ is the fraction of the adsorbed sites at a pressure P and temperature T, R is the universal constant. The equation can be further derived as following expression for transitions between a gas and a condense phase.

$$ln\ P_2 - ln\ P_1 = \frac{Q}{R}\left(\frac{1}{T_1} - \frac{1}{T_2}\right) \quad (3)$$

Supplementary Note 3. Detailed discussion for the ^{13}C NMR assignments.

The three NMR spectra in Figure 3d were obtained under identical conditions: 12 kHz MAS, 2.5-μs 90° ^{13}C pulse, 41-ms FID, 10-s relaxation delay; 480 scans; 50 Hz of line broadening applied to the FID.

Numerous MAS NMR investigations of CO_2 have reported a signal at 125 ± 1 ppm, regardless of the physical environment for the CO_2: free gas, physisorbed on various materials, in a metal organic framework, in a clathrate, dissolved in a glass, etc.[7-20] Accordingly, attributing the signal at 130.6 ppm to CO_2 physisorbed on the sorbent seems reasonable, although the reason for the additional deshielding is not obvious. This 5-ppm difference does not result from the use of different chemical shift references, as the various reports indicate that either the signal from $Si(CH_3)_4$ (TMS) serves as the chemical shift reference (0 ppm)[7-9,12,13] or that the signal from a solid such as adamantane[15,19,20] or glycine (this work) relative to TMS at 0 ppm[21] serves as the chemical shift reference. We note that the sorbent is somewhat conductive in that it has a

noticeable effect on the tuning and matching of the ^{13}C and ^{1}H channels of the NMR probe (relative to the tuning and matching for glycine); however spinning is unaffected.[22-25] Perhaps the somewhat conductive nature of the sorbent results in the 5-ppm deshielding effect observed for physisorbed CO_2.

A chemical shift of 166.5 ppm is rational for poly(CO_2) in light of various reports of bicarbonate and carbonate species giving signals from 162 to 170 ppm[14,26-29] relative to TMS[26-27] or to $[(CH_3)_3Si]_4Si$[28-29] which is 3.5 ppm relative to TMS at 0 ppm.[21] The carbonyl chemical shift of CH_3O-CO-O-CO-OCH_3 is extremely sensitive to its environment: the reported shift is 147.9 ppm as a neat liquid at 37°C[30] and 157 ppm in $CDCl_3$, both relative to TMS.[31] We are not aware of any reports of chemical shift data for poly(CO_2) and are hereby reporting the first such example of that chemical shift at 166.5 ppm when entrapped in this carbon matrix.

Supplementary References

1. Mason, J. A., Veenstra, M. & Long, J. R. Evaluating metal–organic frameworks for natural gas storage. *Chem. Sci.* **5**, 32-51 (2014).
2. Hartzog, D. G. & Sircar, S. Root surface area measurements based on adsorption and desorption of nitrite. *Adsorption* **175**, 133-137 (1995).
3. Y. Xia, Y. Zhu, Y. Tang, Preparation of sulfur-doped microporous carbons for the storage of hydrogen and carbon dioxide. *Carbon* **50**, 5543-5553 (2012).
4. Guo, B., Chang, L. & Xie, K. Adsorption of carbon dioxide on activated carbon. *J. Natural Gas Chem.* **15**, 223-229 (2006.)
5. Auerbach, S. M., Carrado, K. A. & Dutta, P. K. *Handbook of Zeolite Science and Technology*, Marcel Dekker, Inc. New York (2003).
6. Zhang, Z. *et al.* Enhancement of CO_2 adsorption and CO_2/N_2 selectivity on ZIF-8 via postsynthetic modification. *AIChE J.* **59**, 2195-2206 (2013).
7. Kohn, S. C., Brooker, R. A. & Dupree, R. ^{13}C MAS NMR: A method for studying CO_2 speciation in glasses. *Geochim. Cosmochim. Acta* **55**, 3879-3884 (1991).
8. Salehirad, F. & Anderson, M. W. Solid-State ^{13}C MAS NMR Study of methanol-to-hydrocarbon chemistry over H-SAPO-34. *J. Catal.* **164**, 301-314 (1996).
9. Jones, C. A., Stec, D. & Larsen, S. C. Magnetic resonance studies of reactions of urea and

nitric oxide on FeZSM-5, HZSM-5 and silicalite. *J. Mol. Catal. A: Chem.* **212**, 329-336 (2004).

10. Omi, H., Ueda, T., Miyakubo, K. & Eguchi, T. Dynamics of CO_2 molecules confined in the micropores of solids as studied by ^{13}C NMR. *Appl. Surf. Sci.* **252**, 660-667 (2005).
11. Frey, J., *et al*. Vanadium phosphates on mesoporous supports: model catalysts for solid-state NMR studies of the selective oxidation of *n*-butane. *Solid State Nucl. Magn. Reson.* **35**, 130-137 (2009).
12. Morizet, Y., Paris, M., Gaillard, F. & Scaillet, B. Raman quantification factor calibration for CO-CO_2 gas mixture in synthetic fluid inclusions: Application to oxygen fugacity calculation in magmatic systems. *Chem. Geol.* **264**, 58-70 (2009).
13. Qian, L., *et al*. Controlled atmosphere ^{13}C and ^{1}H MAS NMR study of reforming route of methane with carbon dioxide over Rh/SBA-15. *Appl. Catal. A: Gen.* **401**, 114-118 (2011).
14. Hoyt, D. W., *et al*. High-pressure magic angle spinning nuclear magnetic resonance. *J. Magn. Reson.* **212**, 378-385 (2011).
15. Lee, J.-W. & Yoon, J.-H. Preferential occupation of CO_2 molecules in hydroquinone clathrates formed from CO_2/N_2 gas mixtures. *J. Phys. Chem. C* **115**, 22647-22651 (2011).
16. Loring, J. S., *et al*. *In Situ* molecular spectroscopic evidence for CO_2 intercalation into Montmorillonite in supercritical carbon dioxide. *Langmuir* **28**, 7125-7128 (2012).

17. Hoffmann, H. C., *et al*. Solid-state NMR spectroscopy of metal-organic framework compounds (MOFs). *Materials* **5**, 2537-2572 (2012).

18. Comotti, A., *et al*. Porous dipeptide crystals as selective CO_2 adsorbents: experimental isotherms *vs.* grand canonical Monte Carlo simulations and MAS NMR spectroscopy. *CrystEngComm* **15**, 1503-1507 (2013).

19. Gul-E-Noor, F., *et al*. Adsorption of small molecules on $Cu_3(btc)_2$ and $Cu_{3-x}Zn_x(btc)_2$ metal-organic frameworks (MOF) as studied by solid-state NMR. *J. Phys. Chem. C* **117**, 7703-7712 (2013)

20. Bowers, G. M., *et al*. *In situ* ^{13}C and ^{23}Na magic angle spinning NMR investigation of supercritical CO_2 incorporation in Smectite-natural organic matter composites. *J. Phys. Chem. C* **118**, 3564-3573 (2014).

21. Hayashi, S. & Hayamizu, K. Chemical shift standards in high-resolution solid-state NMR (1) ^{13}C, ^{29}Si, and ^{1}H nuclei. *Bull. Chem. Soc. Jpn.* **64**, 685-687 (1991).

22. Solum, M. S., Sarofim, A. F., Pugmire, R. J., Fletcher, T. H. & Zhang, H. ^{13}C NMR analysis of soot produced from model compounds and a coal. *Energy Fuels* **15**, 961-971 (2001).

23. Jiang, Y. J., *et al*. A new method for measuring the graphite content of anthracite coals and soots. *Energy Fuels* **16**, 1296-1300 (2002).

24. Gao, W., Alemany, L. B., Ci, L. & Ajayan, P. M. New insights into the structure and reduction of graphite oxide. *Nat. Chem.* **1**, 403-408 (2009).

25. Genorio, B., *et al*. *In Situ* intercalation replacement and selective functionalization of graphene nanoribbon stacks. *ACS Nano* **6**, 4231-4240 (2012).

26. Papenguth, H. W.; Kirkpatrick, R. J., Montez, B. & Sandberg, P. A. ^{13}C MAS NMR spectroscopy of inorganic and biogenic carbonates. *Amer. Mineral.* **74**, 1152-1158 (1989).

27. Lazo, N. D., Murray, D. K., Kieke, M. L. & Haw, J. F. *In situ* carbon-13 solid-state NMR study of the $Cu/ZnO/Al_2O_3$ methanol synthesis catalyst. *J. Amer. Chem. Soc.* **114**, 8552-8559 (1992).

28. Kwak, J. H., *et al*. Metal carbonation of forsterite in supercritical CO_2 and H_2O using solid state ^{29}Si, ^{13}C NMR spectroscopy. *J. Phys. Chem. C* **114**, 4126-4134 (2010).

29. Kwak, J. H., *et al*. The role of H_2O in the carbonation of forsterite in supercritical CO_2. *Int. J. Greenhouse Gas Control* **5**, 1081-1092 (2011).

30. Olah, G. A., Halpern, Y., Westerman, P. W. & Grant, J. L. Stable carbocations. CLXVIII. protonation and cleavage of dialkyl pyrocarbonates in FSO_3H-SbF_5 (magic acid)-SO_2 solution. *J. Org. Chem.* **39**, 2390-2393 (1974)

31. BioRad ^{13}C spectrum ID NC_28161 accessed *via* SciFinder Scholar on March 18, 2014.